J. Fluid Mech. (1993), *vol.* 249, *pp.* 391–414

Experiments on liquid mixing and reaction in a vortex

By BAKI M. CETEGEN AND NAZRI MOHAMAD
Mechanical Engineering Department, University of Connecticut, Storrs, CT 06269-3139, USA

(Received 30 July 1991 and in revised form 3 June 1992)

A series of experiments were conducted in water to study mixing in the field of a single, two-dimensional vortex. The experimental configuration is that of a laminar line vortex initiated along a diffusion layer between two streams of different scalar concentrations. Measurements of passive scalars in inert and chemically reactive environments were made using a planar laser-induced fluorescence technique. A fast acid/base isothermal reaction was utilized to highlight the molecular mixing. The experimental results show that the mixing enhancement in the presence of a vortex is linearly dependent on the vortex strength and the time elapsed since vortex initiation. In particular, the mixedness, defined as the spatially integrated second moment of concentration field in the vortex, and the spatially averaged scalar dissipation are found to follow this dependence. This variation is mainly attributed to the contact area generation along the diffusion layers between the two streams as a result of inviscid deformations in the vortical flow field. The results presented pertain to mixing in liquids and in the limit of high Schmidt numbers.

1. Introduction

Turbulent flows have been extensively studied in the past several decades to understand the underlying physics of mass, momentum and energy transport and their mutual interactions. The fundamental studies have ranged from purely experimental investigations of jets, mixing layers and other prototypical flows to their analytical/numerical simulations. A unified fundamental understanding of turbulent mixing has been slowly emerging through these efforts. The study of turbulent flows is, in general, complicated by its multiscale character and the nonlinear dynamics determining the interactions among all scales. One distinct feature of many turbulent flows is, however, their large-scale organization in the form of vortical structures (Brown & Roshko 1974). These large-scale structures have been shown to exist in flows of very large scales and high Reynolds numbers (Mungal & Hollingsworth 1989).

The role of these large-scale vortical structures in mixing has been studied extensively. In particular, mixing in chemically reacting flows has been of special interest in the fields of chemical engineering and combustion. This interest mainly stems from the fact that chemical reactions take place upon molecular diffusion of reactants into one another whereas the mechanical stirring process begins at scales associated with large eddies in a turbulent flow field. In a sequence of cascading events, stirring at large scales progressively creates smaller scales due to continuous stretching and folding, ultimately tending to a state of complete mixing in the presence of molecular diffusion along the stretching interfaces between mixing fluids. To understand the interplay between flow kinematics and mixing, it has been found useful to study the influence of deformations across segregated fluid interfaces with diffusion

and chemical reaction in laminar flow fields which possess some of the main characteristics of local turbulent flow structures. This approach has been advanced by a number of reseachers. Most notable among them are the works of Ranz (1979), Ottino (1982, 1989) and their coworkers who studied kinematics of mixing in small-scale prototypical flows, and the combustion studies of Marble & Broadwell (1977), Carrier, Fendell & Marble (1975) and Fendell (1965) in vortical and lammelar structures.

One of the problems which has received considerable attention in connection with mixing in turbulent flows is the interaction of a laminar vortex with a diffusion–reaction interface between two fluids. Ranz (1977), Ottino (1982), Marble (1985) and Karagozian & Marble (1986) have carried out theoretical analyses on this problem. The mixing in the field of a vortex takes place due to the distortion of diffusion zones between fluids by the vortical convective motion increasing the contact area between them and as a result of enhancing the mass transfer rate across these regions via stretching. For instance, Marble (1985) has analytically studied the interaction of a two-dimensional laminar viscous vortex with a diffusion flame and demonstrated the effects produced by this interaction in terms of reactant consumption and combustion enhancement. This problem has since received considerable attention and other studies on similar problems have been reported by Laverdant & Candel (1989), Peters & Williams (1988), Rehm *et al.* (1989) and Cetegen & Sirignano (1990).

This article concerns an experimental study of mixing and chemical reaction in a laminar isolated vortex generated along a diffusion layer in water as a useful subelement to develop a clearer understanding of turbulent mixing. The main objective is to characterize the vortical mixing enhancement as a function of vortex circulation and time of vortex evolution. This experiment differs from the spatial mixing-layer studies where a trail of vortical stuctures is generated as a consequence of the shear-layer instability. Mixing-layer structures typically grow and interact with one another due to pairing downstream in the layer. In the experiments reported, single laminar vortices with measurable circulation and time of evolution were generated to characterize mixing of two fluids with different scalar concentrations residing on the opposite sides of the vortex. In addition to the presentation of new experimental results, this study provides an experimental basis against which the earlier theoretical results can be compared. The evolution of non-reacting and reacting scalar distributions within vortices is investigated using laser diagnostics. In particular, emphasis is placed upon mixing at the molecular scale that controls the rates of diffusion-limited chemical reactions. The experimental results are discussed in terms of several mixing parameters and mixing statistics. In the following sections, we describe the vortex generation technique, the experimental methods and the experimental results. The article concludes with a summary of the key findings.

2. Generation and characterization of isolated vortices

The main objective of this study is to quantify mixing in the field of an isolated laminar vortex coincident with a diffusion layer as a function of time of interaction and vortex strength. A series of vortex generation schemes at a diffusion layer were considered, as discussed in detail by Mohamad (1991). Among these, for example, was the mixing of two fluids around a rotating cylinder. Although interesting in its own right, this scheme produces a purely viscous flow field. It is, however, well recognized that large-scale structures are produced inviscidly in many turbulent flows. The examination of an inviscidly generated vortex that subsequently decays due to viscosity

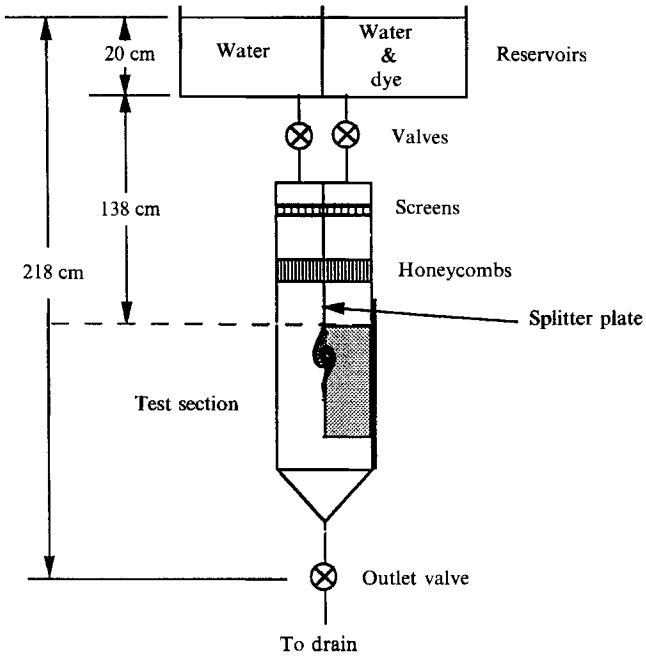

FIGURE 1. Experimental apparatus.

was therefore preferred. A simple way of generating a single vortex coincident with a diffusion layer in water was achieved in a gravity-fed mixing layer apparatus as shown in figure 1. Two liquid streams (water and water premixed with dye) of equal velocity were brought together at the end of a splitter plate forming a laminar diffusion layer. At these low velocities, the interface was found to be very stable and straight before vortex initiation, as shown in the top picture of figure 2. Generation of the vortex was facilitated by retarding the flow rate of one of the streams for a short period of time, thus initiating the roll-up of a single vortical structure at the trailing edge of the splitter plate. As the vortex convected downstream (from right to left in figure 2), it grew in size and the number of windings in the vortex centre increased.

In this configuration, the vortex strength could be quantified either by determining the flow rate pulse characteristics or by measuring the growth of the generated vortices. In the former case, measured flow pulse characteristics and the wake thickness behind the splitter plate can be related to the vortex circulation. However, a more straightforward approach was taken here involving the measurement of the lateral growth rate of the generated vortices. This method was found to be advantageous from the standpoint that there is no need for elaborate instrumentation for the pulse characterization. On the other hand, it had the disadvantage that the vortex strength can only be determined *a posteriori*. The main assumption here is that the growth of the generated vortex conforms to that of a decaying viscous line vortex described by the velocity field (cf. Batchelor 1967);

$$V_r = \frac{\mathrm{d}r}{\mathrm{d}t} = 0, \quad V_\theta = r\frac{\mathrm{d}\theta}{\mathrm{d}t} = \frac{\Gamma}{2\pi r}\left[1-\exp\left(-\frac{r^2}{4\nu t}\right)\right], \tag{1}$$

where r is the radius from vortex centre and θ is the angular displacement taken here in the counterclockwise direction from positive horizontal axis, Γ is vortex circulation, t is time and ν is the kinematic viscosity. The first equation states that the pathlines are

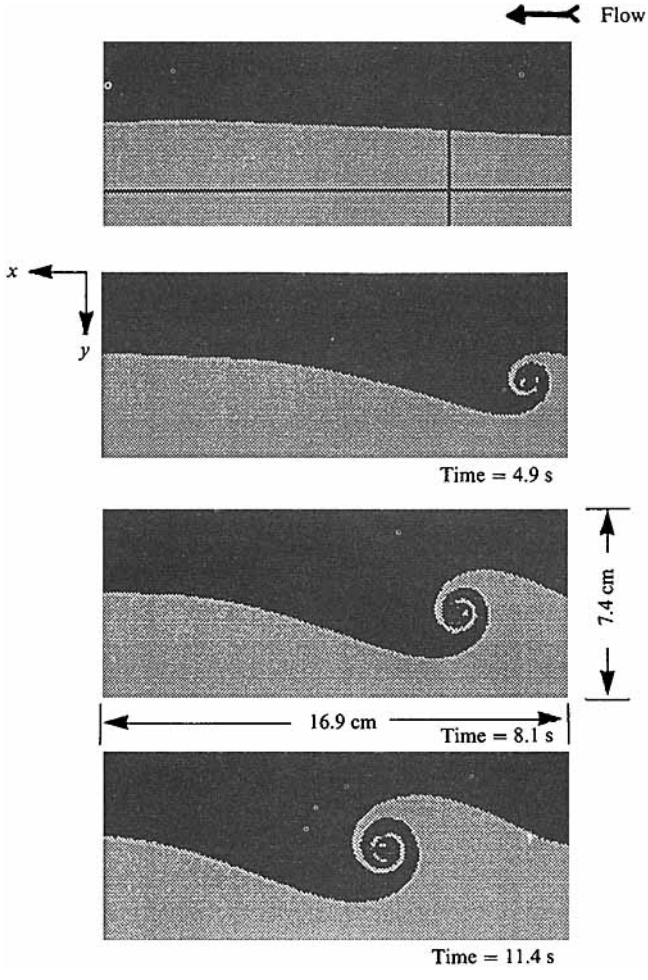

FIGURE 2. Evolution of a two-dimensional vortex convecting downstream in the test section.

circular. The angular positions of the fluid elements lying at constant radii can be found by integration of the second equation with respect to time. This integration yields a relationship between the circulation of the generated vortex or a non-dimensional parameter called here the Reynolds number, $R = \Gamma/2\pi\nu$, the angular position, θ and a non-dimensional parameter, $\eta = r^2/4\nu t$. When the resulting expression is evaluated for the vertical extent of a vortex initiated at the trailing edge of the splitter plate by imposing the condition $r_*(\theta = \frac{1}{2}\pi)$ at a time $t_* = x_*/U_c$, it becomes

$$R = \frac{2\pi}{\dfrac{1-e^{-\eta_*}}{\eta_*} + \displaystyle\int_{\eta_*}^{\infty} \frac{e^{-\eta}\,d\eta}{\eta}} \tag{2}$$

which simplifies for a potential vortex, or when $r_*^2 \gg 4\nu t_*$, to

$$R = 2\pi\eta_* = \pi r_*^2/2\nu t_* \quad \text{or} \quad \Gamma = (\pi r_*)^2/t_*. \tag{3}$$

The vortex evolution time is related to the convection velocity by $t_* = x_*/U_c$, where x_* is the downstream distance measured from the slitter plate tip to the vortex centre and U_c is the convection velocity of the vortex. $2r_*$ is the vortex size in the direction normal to that of vortex convection. Measurements of r_* and t_* provide a means for

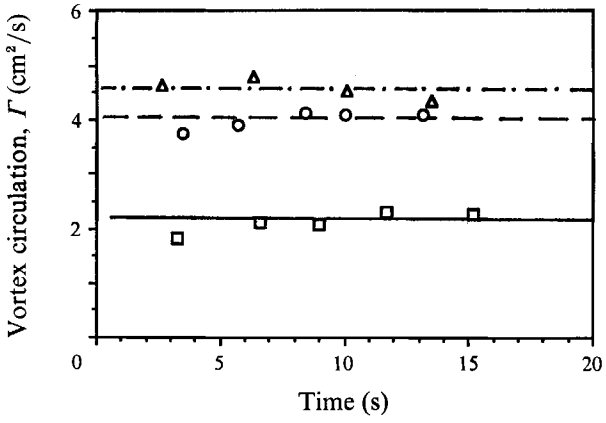

FIGURE 3. Computed vortex strength as a function of time: □, non-reacting (average = 2.22 cm²/s); ○, non-reacting (average = 4.05 cm²/s); △, reacting (average = 4.59 cm²/s).

calculating the vortex circulation Γ from second of equation (3) in the inviscid region. Figure 3 shows the calculated vortex circulation as a function of time for several vortices. The vortex strength remains approximately constant during the vortex advection until it grows large and begins to interact with the walls of the test section. Since the initial roll-up of the vortex is essentially inviscid, we adopt here the vortex circulation as a measure of vortex strength as opposed to the vortex Reynolds number mentioned earlier.

3. Scalar concentration measurements by planar laser-induced fluorescence

The planar laser-induced fluorescence (PLIF) technique was used to quantify the scalar concentration field using a dilute fluorescent dye solution (6×10^{-7} M) as one of the streams. An organic dye, disodium fluorescein salt ($C_{20}H_{10}O_5Na_2$) was used as a fluorescent tracer. When excited by the blue ($\lambda = 488$ nm) light from an Ar^+ laser, fluorescein dye fluoresces in the green peaking around $\lambda = 514.5$ nm. Two types of experiments (dilution and chemically reacting experiments) were conducted to quantify mixing within vortices.

3.1. *Concentration measurements based on dilution*

In this experiment, the fluorescent dye (a passive scalar) was present in one of the two water streams in the mixing-layer apparatus and its mixing with the other stream of pure water was studied. The fluorescence from the local dye solution environment was used to monitor the local scalar concentrations. At very dilute free-stream dye concentrations and low light excitation levels, the fluorescence intensity becomes proportional to the dye concentration, as shown in figure 4(*a*). Thus, a quantitative measurement of the local dye concentration can be accomplished by measuring the fluorescence intensity. The relation between the concentration and the locally measured fluorescence intensity is given by

$$C_d/C_{d0} = I_f/I_{fmax}, \tag{4}$$

where C_d is the local dye concentration, C_{d0} is the free-stream dye concentration carried by the dye stream, I_f is the local fluorescence intensity and I_{fmax} is the fluorescence intensity corresponding to the free-stream dye concentration. The local normalized dye concentration ξ in the sampling volume is given by

$$\xi = C_d/C_{d0} = v_2/(v_1+v_2) = I_f/I_{fmax}, \tag{5}$$

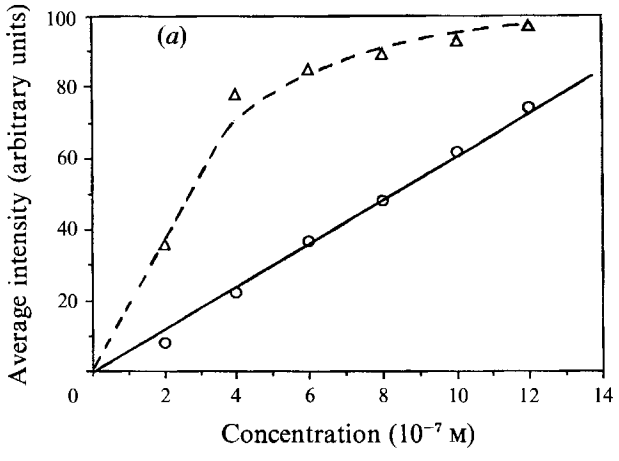

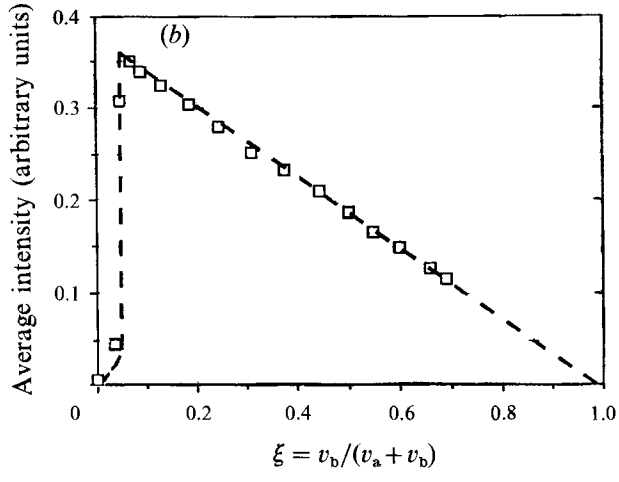

FIGURE 4. Fluorescence intensity calibrations. (*a*) Average intensity versus dye concentration at two laser power settings (○, 0.2 W; △, 1.2 W); (*b*) average intensity versus base volume fraction in chemically reacting fluorescence tests, 5×10^{-4} M H_2SO_4, 1.5×10^{-2} M NaOH, laser power 10^{-2} W, PM voltage 520 V.

where v_1 and v_2 are respectively volumes of fluid from pure water and water/dye streams in the sampling volume and ξ is the normalized concentration which varies from zero for the pure water to one for the dye stream.

3.2. *Concentration measurements based on chemical reaction*

In the dilution measurement technique, detection of molecular diffusion (often referred to as molecular mixing) is hindered typically by the disparity between the measurement resolution and the smallness of the molecular diffusion scale. For example, the spatial resolution dictated by the optics (0.34 mm in the object plane in our experiments) is much lower than that required to capture molecular diffusion layer thickness (e.g. diffusion-layer thickness, $\sqrt{4Dt}$, in water is 0.1 mm for $t = 1.0$ s). When the spatial resolution of the measurements is less than that to detect molecular diffusion, it becomes impossible to distinguish whether the two fluids are molecularly mixed within the spatial measurement resolution. Optical measurements only provide an average

concentration up to the optical resolution scale. Although the passive scalar technique yields an upper bound to the actual molecular mixing as discussed by Koochesfahani & Dimotakis (1986), this technique requires modification to quantify the degree of molecular diffusion.

The modified technique is based on the pH sensitivity of fluorescence from disodium fluorescein dye as described by Breidenthal (1981). A fast isothermal chemical reaction between slightly acidic and basic water streams with the fluorescent dye premixed in the acidic stream can be utilized to highlight molecular mixing. The fluorescence behaviour of the dye depends on the local chemical environment surrounding it. It fluoresces efficiently when excited by an Ar^+ laser light with a wavelength of $\lambda = 488$ nm, provided that it is in a solution whose pH is above the threshold value of about 4. The fluorescence is suppressed if the dye molecule is in a solution below this pH threshold. The volume of base, v_b required to titrate a unit volume of acid, v_a to cross the pH threshold can be adjusted by proper choice of the free-stream acid and base concentrations. Figure 4(*b*) shows the fluorescence intensity variation in the acidic solution (5.0×10^{-4} M H_2SO_4 in H_2O) premixed with the fluorescein dye titrated with a basic solution (1.5×10^{-2} M NaOH in H_2O). Initially, the pH of the acid solution is below the threshold, therefore no fluorescence takes place. Addition of more base causes no significant increase in fluorescence intensity until the threshold pH is crossed, when the intensity sharply rises to its maximum value. Beyond this point, further addition of base merely dilutes the dye solution and the fluorescence intensity becomes a linearly decreasing function of the dye concentration proportional to the base volume fraction ($\xi = v_b/(v_a+v_b)$). Since the product is formed upon molecular mixing of the two streams, the observed fluorescence intensity is directly proportional to the product concentration, where chemical product is defined here as the dye-bearing fluid whose local pH is above the fluorescence threshold. The local instantaneous product concentration, C_p, normalized with its maximum possible value C_{pmax} at the threshold condition for the fluorescence 'turn-on', is given by

$$C_p/C_{pmax} = I_f/I_{fmax}, \tag{6}$$

where I_f is the measured fluorescence intensity and I_{fmax} is its maximum possible value reached at the fluorescence threshold conditions. The definition of the product concentration in terms of the fluorescence intensity is not entirely arbitrary and is closely connected with the distribution of the product concentration in a fast irreversible chemical reaction as explained by Koochesfahani & Dimotakis (1986).

For the PLIF experiment using acid–base reaction with fluorescent dye premixed in the acid solution, the product concentration is given by

$$C_p(\xi;\xi_s) = 0 \quad \text{for} \quad \xi < \xi_s, \tag{7a}$$

$$C_p(\xi;\xi_s) = C_{d0}(1-\xi) \quad \text{for} \quad \xi > \xi_s, \tag{7b}$$

where $\xi_s = [v_b/(v_a+v_b)]_{thr}$ is the base volume fraction at the threshold condition for fluorescence 'turn on' and C_{d0} is the free-stream dye concentration carried by the acid solution. In the reported experiments, ξ_s had a value of 0.05. Combining (6) and (7*b*), one gets

$$C_p/C_{pmax} = I_f/I_{fmax} = (C_{d0}/C_{pmax})(1-\xi) \quad \text{for} \quad \xi_s < \xi < 1. \tag{8}$$

Since the base volume fraction at the threshold is small, it can be assumed negligible at the point of maximum intensity I_{fmax} such that $C_{d0} = C_{pmax}$. The base volume fraction can then be written as

$$\xi = 1 - I_f/I_{fmax}, \tag{9}$$

where I_f and I_{fmax} are experimentally measured intensities. Therefore, measurements of

I_f and $I_{f\max}$ facilitate determination of molecularly mixed base volume fractions. These measurements provide information on molecular mixing at infinite resolution since only the molecularly mixed fluid can be detected with this technique. The spatial resolution dictated by the optical set-up remains the same as in the dilution experiments. This implies that the detected molecular mixing is still spatially averaged within the optical resolution. This averaging, however, does not severely affect the measures of molecular mixing discussed later.

In both dilution and chemical reaction PLIF measurements, the raw images of fluorescence intensity need to be first processed for non-uniformities in laser illumination as well as the incident light absorption by the fluorescent dye to obtain quantitative measures of concentration field. A series of calibration experiments and digital image manipulations were performed to account for these effects, as described by Mohamad (1991).

4. Description of experimental systems

4.1. *Apparatus*

Vortices were generated using the procedures described earlier in a vertical channel made out of Plexiglas with a cross-section of 12 by 14 cm and 70 cm in length, in which two liquid streams (water and water mixed with dye) were brought together at the end of a thin brass splitter plate (0.2 mm thickness) as shown in figure 1. Each stream of fluid was gravity fed from two reservoirs 138 cm above the test section as measured from the trailing end of splitter plate. The splitter plate divided the channel into two equal cross-sections. The water velocities on either side of the splitter plate were equal since both channels were fed from two identical reservoirs filled to identical heights connected by identical piping. Each stream originated from a reservoir and passed through a valve followed by flow straightening devices (PVC screens and honeycombs) before reaching the end of the splitter plate. Since the experiments were conducted at low velocites (typically of the order of 1 cm/s) these flow management schemes proved adequate to yield uniform velocity profiles at the entrance of the test section. At the exit of the channel, there was a short contraction section connected to an exit valve. The purpose of this downstream valve was to control the flow rates of both streams simultaneously by regulating the outlet flow rate. An LED digital chronometer was placed in viewfield of the camera to record the time during the experiments.

The flow rate pulse was generated by closing and re-opening of one of the upstream valves which were otherwise kept fully open during the tests. This operation was performed in two different ways in the course of our experiments. The first one involved pneumatic rotation of a sponge-padded plate covering the drain hole in one of the reservoirs. The other utilized the hand operation of one of the upstream valves. After some experience, the vortex generation was best achieved by the hand operation. The vortex strength was varied by changing the velocity of the two streams along with the flow rate pulse duration. The variation of the convection speed of a vortex during its travel due to the variation of the free-surface height in the reservoirs was estimated to be typically less than 1% of the initial vortex convection speed.

In the acid–base chemical reaction experiments, maintaining a stable straight interface between the streams was difficult due to the small density mismatch. This was overcome by adding the appropriate amount of Na_2SO_4 into the acid solution to match the densities of the two streams.

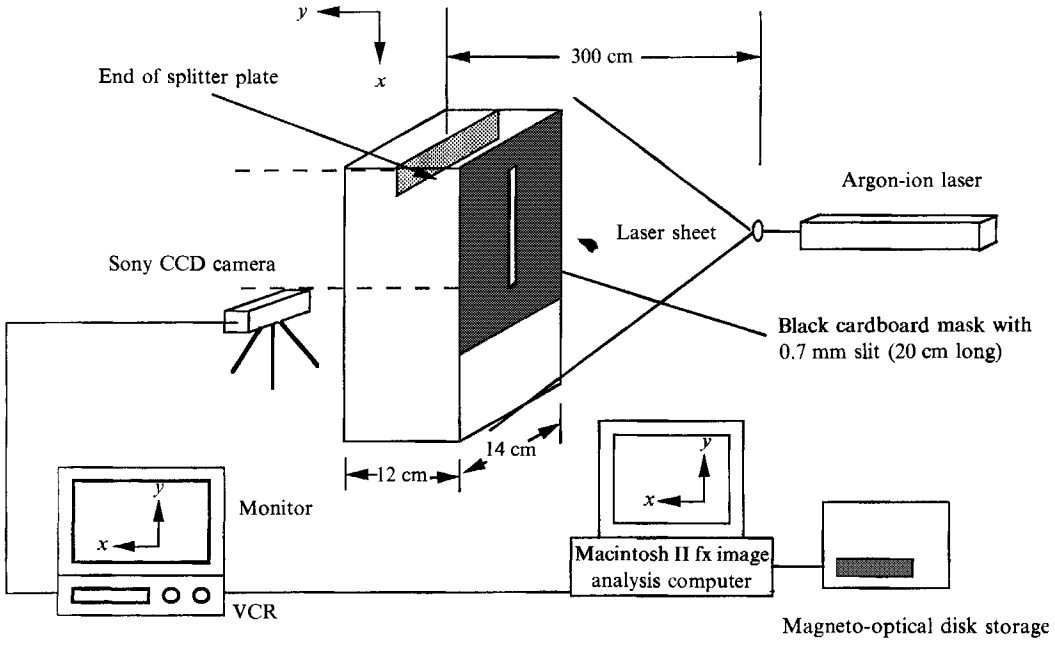

FIGURE 5. Schematics of experimental set-up and data acquisition systems.

4.2. *PLIF measurements set-up*

The optical set-up for the PLIF experiments is shown in figure 5. The beam of an Ar^+ laser (Coherent Innova 90-6) at a wavelength of 488 nm was formed into a sheet using a 500 mm focal length concave cylindrical lens. The light sheet thickness was reduced to 0.7 mm by a slit. The two-dimensional fluorescence from the convecting vortex was viewed by a 480×640 pixel array B&W CCD camera (Sony, SSC-D7). Each pixel of the CCD array received light from a small area in the object plane 0.34×0.34 mm when the camera was positioned at a distance of 40 cm from the imaging plane. The camera position was unchanged during the calibrations and the experiment. At this distance, the field of view of the camera covered an area of 16 by 22 cm at the object plane. The camera position was chosen such that the growing vortex was seen in its entirety until it was convected about 17 cm downstream of the splitter plate. One of the difficulties was the scattering of laser light by small particles and micro air bubbles in water although the reservoir fluids were thoroughly filtered. An orange photographic filter (Wratten no. 16) successfully blocked any scattered light. Although this filter lowered the fluorescence intensity slightly due to absorption in the fluorescence band, it helped to significantly reduce any scattered light at the incident wavelength of $\lambda =$ 488 nm. The fluorescence images were recorded on videotape for subsequent image digitization and processing on a Macintosh II fx computer. The digitized images were also stored on a magneto-optical disk (Third Wave Computing) for further analysis using optical multichannel analysis software.

5. Results and discussion

The experimental results are presented in this section for the non-reacting and the reacting vortices. The general characteristics of the experimentally generated vortices are first briefly discussed. A quantitative analysis of mixing is given for the vortices

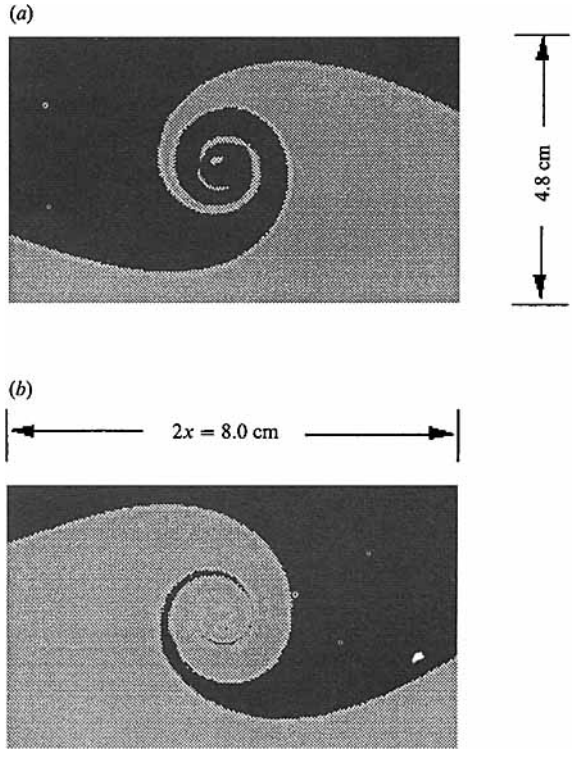

FIGURE 6. Comparison of concentration field between (*a*) penetrated and (*b*) penetrating fluid with dye. (*a*) $\Gamma = 3.05$ cm^2/s, $t = 11.4$ s; (*b*) $\Gamma = 2.99$ cm^2/s, $t = 11.6$ s.

studied in terms of several measures of mixing such as mixedness, mean scalar concentrations, probability density functions and scalar dissipation.

In the vortex initiation process, the flow rate of one of the two streams was pulsed to initiate the rollup of a vortex as described earlier. During this period, a tongue of fluid from the higher velocity stream penetrated towards the other side and the subsequent roll-up took place around this fluid parcel leaving an excess amount of the high-speed fluid entrapped in the vortex core. In contrast, the theoretical investigations maintain perfect antisymmetric entrainment since the vortex is initiated exactly on the interface between the two fluids, resulting in a vortex core consisting of equal proportions of fluids from both sides. In the experiments, an excess of the fluid from one stream existed in vortex cores depending on the manner the vortex was initiated. In the case that the flow rate of the dye-bearing stream was pulsed, the pure water stream penetrated towards the dye stream as shown in figure 6(*a*). Here, this case will be referred to as 'penetrated fluid with the dye'. On the other hand, if the vortex was initiated by a flow rate depression on the pure water stream, penetration of the dye-containing stream took place as shown in figure 6(*b*). This case is referred to as 'penetrating fluid with the dye'. In a similar fashion, the chemical reaction experiments are distinguished as 'penetrating fluid with the acid-dye' and 'penetrated fluid with the acid-dye'. Although the core fluid concentration is biased as a result of this effect, the rate of mixing in the vortical structure is practically unaffected since mixing predominantly takes place around this initial core.

FIGURE 8. False colour-coded two-dimensional laser-induced-fluorescence images of a vortex at t=10.5 s : effect of vortex strength, *(a)* Γ =2.22 cm^2/s, *(b)* Γ =3.70 cm^2/s.

FIGURE 7. False colour-coded two-dimensional laser-induced-fluorescence images of a vortex of strength Γ =3.05 cm^2/s : time evolution, *(a)* t=8.1 s, *(b)* t=14.8 s.

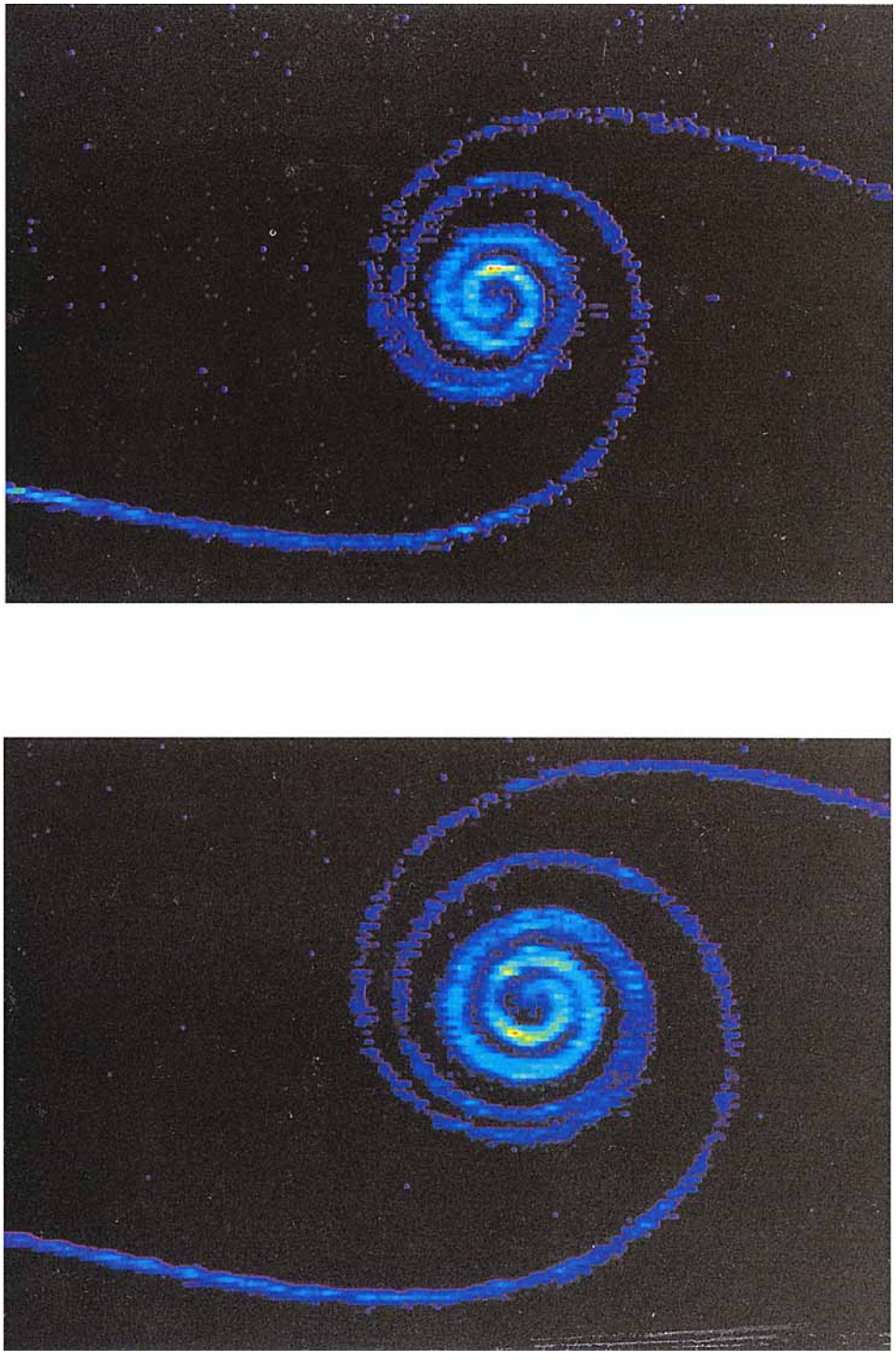

FIGURE 17. False colour-coded, two-dimensional laser-induced-fluorescence images of a chemically reacting vortex of strength Γ =3.99 cm^2/s at two instants of time : *(a)* t=5.9 s, *(b)* t=9.3 s.

5.1. *Dilution experiments*

Spatial distributions of a passive scalar in two-dimensional vortices are presented in this section. Figures 7 and 8 (plate 1) show colour-coded background-corrected concentration distributions as a function of time and vortex circulation respectively. Since the fluorescence intensity is linearly proportional to the fluorescent dye concentration, the images portray the concentration distributions, where red and black correspond to the two free-stream fluids with and without the dye respectively. In figure 7, the concentration field in a vortex with a circulation of $\Gamma = 3.05$ cm^2/s is depicted at two instants. The number of vortex windings, its size and the thickness of the diffusion zones along the vortex arms increase with time. It should be noted that vortex cores are deficient of the dye-bearing fluid since the dye stream was pulsed to generate these vortices. The effect of increasing the vortex circulation at one instant is shown in figure 8. The increasing vortex circulation results in an increase in the number of vortex windings for the same period of time. The structures of lower-circulation vortices at long times and higher-circulation vortices at short times appear similar. Several concentration profiles along the convection path of the vortex (x-direction) at different y-locations are shown in figure 9. These concentration profiles show sharp variations of scalar concentration between adjacent stratifications within the vortex typical of liquids with high Schmidt numbers ($Sc = \nu/D$ where ν is the kinematic viscosity and D is the mass diffusivity). At these experimental conditions, the Schmidt number of water was about 600.

5.1.1. *Measures of scalar concentration distributions*

The measured scalar concentration distributions were utilized to evaluate probability density functions (p.d.f.) and the spatially averaged concentrations in vortical structures to delineate mixing field characteristics.

The p.d.f. of a passive scalar is one of the measures commonly used in turbulent flows to display temporal/spatial characteristics of concentration fields. For instance, in mixing-layer studies, the p.d.f. is obtained from concentration histories measured at locations spanning the thickness of the mixing layer at fixed streamwise positions. In a manner similar to the convection of vortical structures in a spatially evolving mixing layer, the p.d.f. can be constructed for these vortices from the concentration distributions, $\xi(x, y)$, under the Taylor frozen-flow hypothesis along the x-direction by evaluating

$$P(\xi; y) = \frac{\sum_i \frac{\Delta x_i(\xi; y)}{\Delta \xi} [(\xi + \frac{1}{2}\Delta\xi) - (\xi - \frac{1}{2}\Delta\xi)]}{2x_{\max}}. \tag{10}$$

In this expression, the fractional regions occupied by concentrations between $\xi - \frac{1}{2}\Delta\xi$ and $\xi + \frac{1}{2}\Delta\xi$ at each y-position in the region $-x_{\max} < x < x_{\max}$ correspond to their probabilities, assuming that the evolution of the concentration field during convection of the structure across this distance is negligible, i.e. high convection velocity. Here, $x_{\max} = 4.0$ cm was chosen to cover the full extent of the largest vortex in this study. The probabilities are normalized such that

$$\int_0^1 P(\xi, y)\, \mathrm{d}\xi = 1. \tag{11}$$

Figure 10 displays the experimentally determined p.d.f.s. Figure 10(a, b) shows the

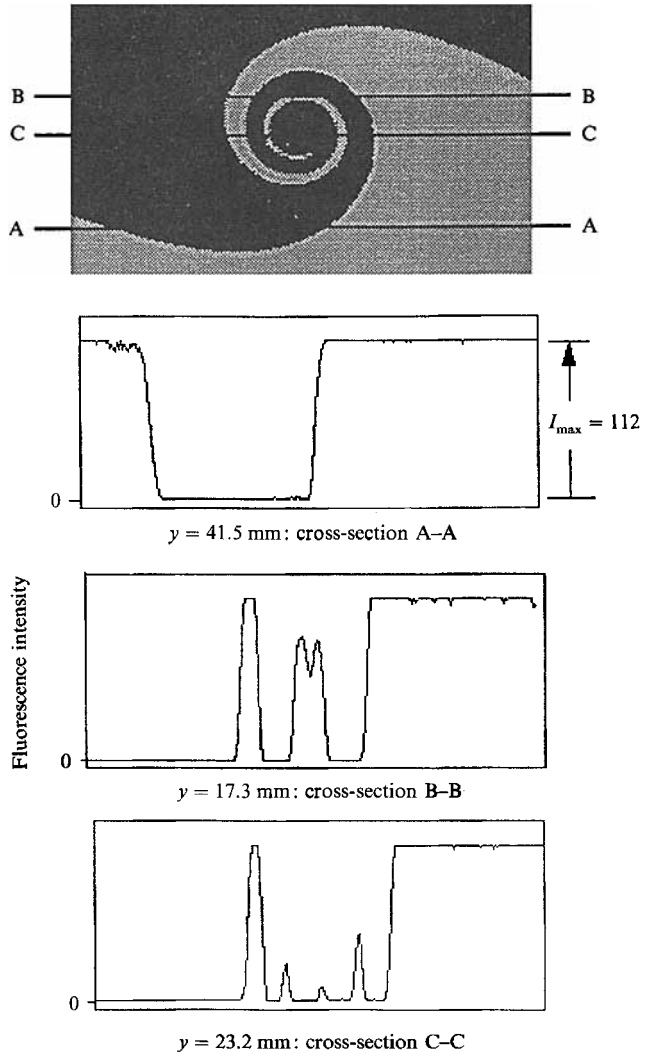

FIGURE 9. Fluorescence intensity profiles along the x-axis at several y-locations for a vortex with $\Gamma = 3.70$ cm^2/s at $t = 10.5$ s.

effect of vortex strength at a fixed time after vortex initiation. The p.d.f. exhibits two distinct peaks at the two limiting concentration values with only small probabilities of mixed fluid in between due to slow molecular diffusion. The particular shapes of the probability peaks at the two limiting concentrations result from the convection of the two fluids in the field of the vortex. It should be noted here that the y-coordinate was scaled with the lengthscale $(\Gamma t/\pi)^{\frac{1}{2}}$ which accounts for the vortex growth with increasing time and circulation. With ageing of a vortex, the probability distributions at the limit concentrations indicate the development of a peak near $\xi = 1$ and a corresponding valley near $\xi = 0$ as shown in figure 10(c, d). At the same time, probabilities at the intermediate concentrations slowly increase. The qualitative features of the experimentally determined p.d.f.s are similar to the computed p.d.f.s (Cetegen & Sirignano 1990) for isolated vortices as well as the p.d.f.s reported by Koochesfahani & Dimotakis (1986) in a liquid mixing layer.

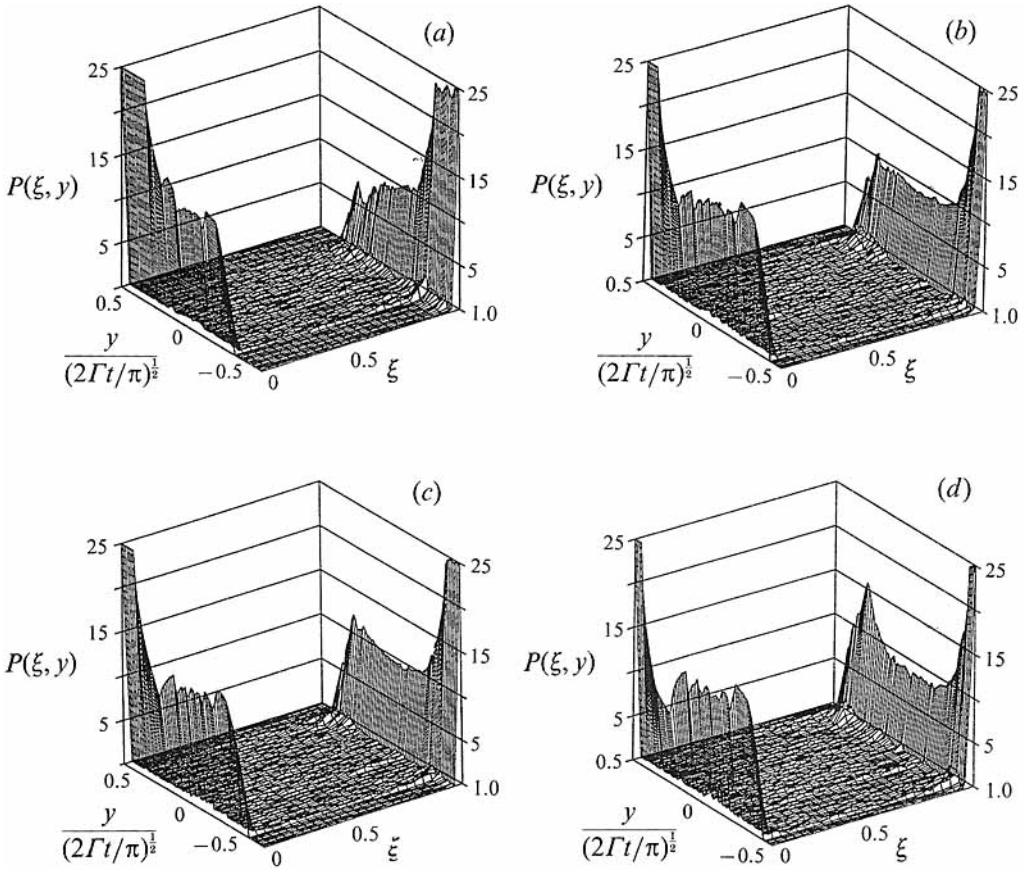

FIGURE 10. Probability density functions of a conserved scalar: (*a*) $\Gamma = 2.22$ cm²/s, $t = 10.5$ s; (*b*) $\Gamma = 3.70$ cm²/s, $t = 10.5$ s; (*c*) $\Gamma = 3.05$ cm²/s, $t = 11.4$ s; (*d*) $\Gamma = 3.05$ cm²/s, $t = 14.8$ s.

The fluid mixture ratio, ξ_m across the vortex in the y-direction can be computed from

$$\xi_m(y) = \int_0^1 P(\xi, y)\, \xi \, d\xi, \tag{12}$$

where ξ_m is mainly a measure of the stirred fluid mixture ratio in the vortical structure. The results are shown in figure 11(*a*) for different times and vortex strengths. The profiles are characterized by steep variations across the outer parts of the vortex with a uniform, zero-gradient core region. Note that although the variations along the outer vortex arms do not appear to change with time and vortex circulation, their dependence is imbedded in the normalization, resulting in variation with $(\Gamma t)^{-\frac{1}{2}}$. In this form, an approximate self-similarity of mixture ratio profiles with $(\Gamma t)^{-\frac{1}{2}}$ is observed, indicating a decrease of 'apparent gradient' with increasing stirring in the vortex. These mixture ratio profiles also show the development of a peak on one side of the vortex with time and increasing vortex circulation caused by the large-scale entrainment of the dye-bearing fluid towards the vortex centre as evident in figures 7 and 8. In addition to these observations, the vortex core concentration has a value of about 0.4, less than the value of 0.5 for the perfectly antisymmetric entrainment from both sides into the vortex core, due to the previously mentioned asymmetry during vortex initiation phase. The results shown in figure 11(*b*) indicate that there is an additional slight increase in the mixture gradient with higher vortex circulation around the outer

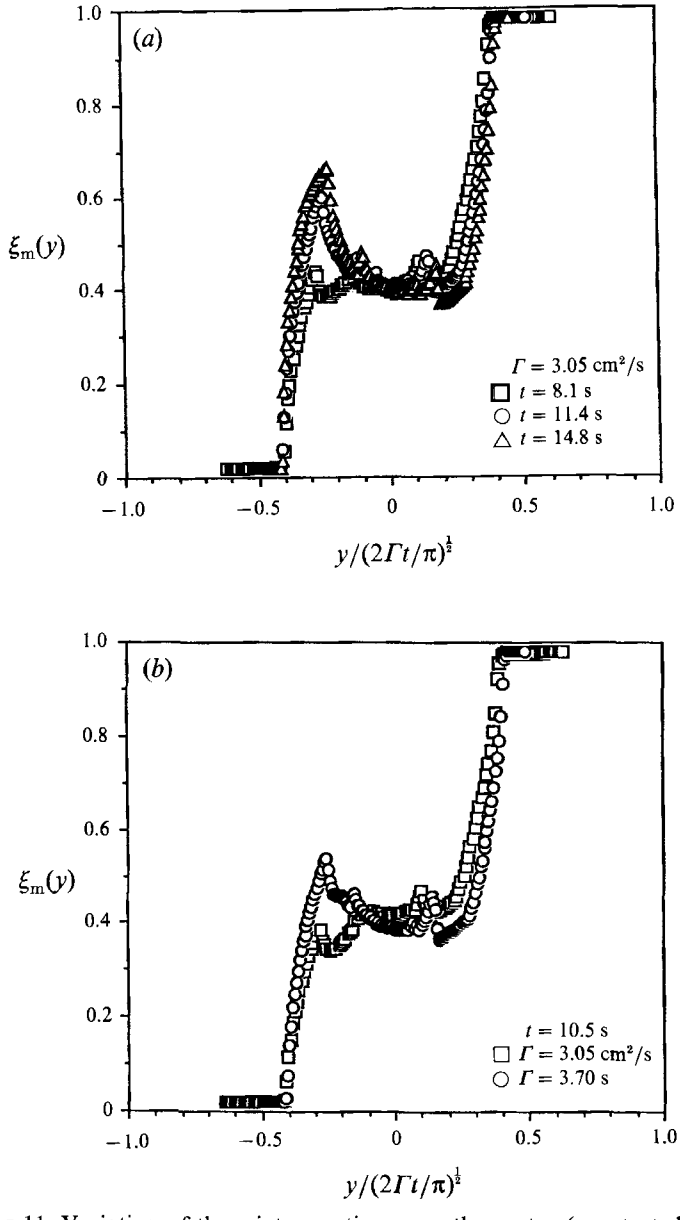

FIGURE 11. Variation of the mixture ratio across the vortex (penetrated fluid with dye): (*a*) effect of time; (*b*) effect of vortex strength.

regions of the vortex which is probably due to the straining of diffusion layers. Figure 12 shows the differences in these distributions for cases where the dye-bearing fluid is either on the penetrating or penetrated sides. The mean concentration in the vortex centre for the penetrating fluid with dye is about 0.56 compared to 0.42 for the penetrated fluid.

The variation of ξ_m with respect to the y-coordinate can be integrated to determine the stirred fluid mixture ratio in the region $-x_{max} < x < x_{max}$ and $-y_{max} < y < y_{max}$:

$$\bar{\xi}_m = \frac{1}{2y_{max}} \int_{-y_{max}}^{+y_{max}} \xi_m(y)\, dy. \tag{13}$$

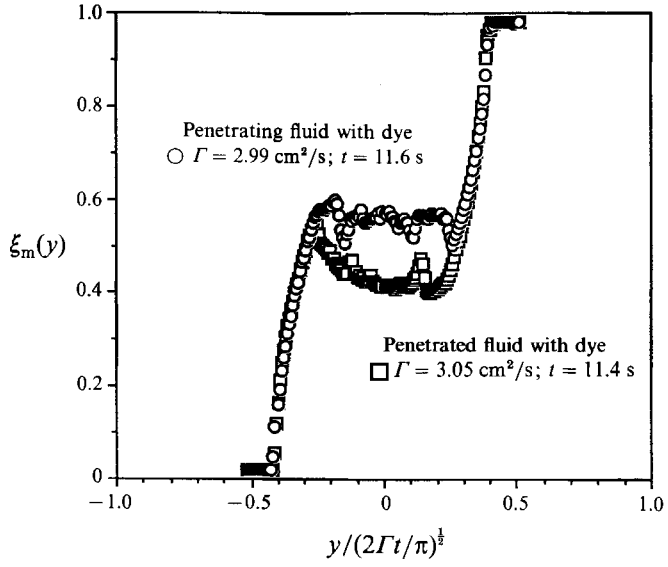

FIGURE 12. Variation of the mixture ratio along the vertical extent of the vortex (penetrated and penetrating fluids with dye).

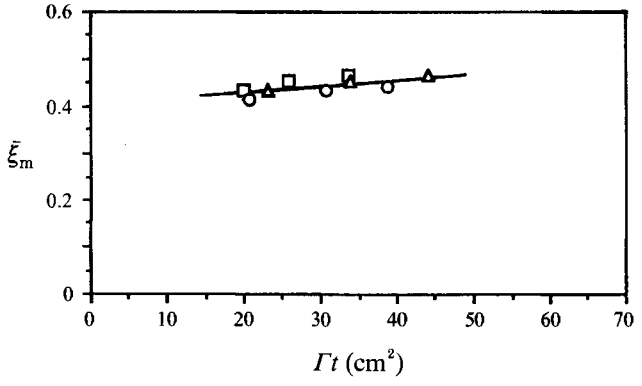

FIGURE 13. Total mixture ratio as a function of vortex circulation–time product, Γt for different vortex strengths: □, $\Gamma = 2.22$ cm²/s; ○, $\Gamma = 3.70$ cm²/s; △, $\Gamma = 4.05$ cm²/s.

This parameter is shown in figure 13 as a function of Γt. It is seen that the variation of $\bar{\xi}_m$ can be correlated well with the parameter Γt for a range of vortex strengths and evolution times. This suggests that the inviscid large-scale dynamics of vortex motion is largely responsible for the stirring process in a vortical structure. The slow increase of $\bar{\xi}_m$ with Γt towards 0.5 is due to the diminishing effect of initial asymmetry with increasing time and vortex strength, as higher equal proportions of two fluids are entrained towards the vortex.

These mixing measures mainly characterize the large-scale inviscid stirring process in a vortical structure. Since the deformation of diffusion layers is predominantly governed by the inviscid rollup, especially for liquid mixing, the vortex circulation–time product parameter Γt is thus found to be relevant in the description of large-scale mixing. These mixing parameters however are not direct measures of the extent of molecular diffusion, or mixedness between two fluids that is important for the progress of chemical reactions. In the following, we concentrate on the descriptions of small-scale mixing.

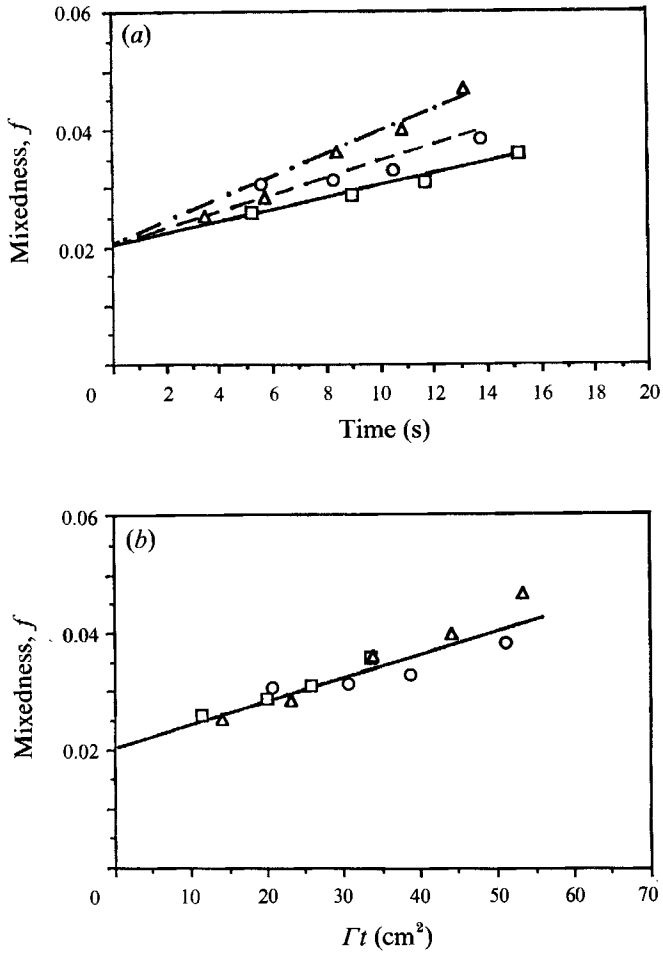

FIGURE 14. Mixedness as a function of (*a*) time and vortex strength and (*b*) vortex circulation–time product, Γt from the dilution experiments: symbols as figure 13.

5.1.2. *Measures of mixedness*

One of the measures of the degree of mixing can be formulated in terms of the second moment of the concentration field, given by

$$f = \frac{4}{A}\int_A \xi(1-\xi)\,\mathrm{d}A. \tag{14}$$

This parameter has a finite value since the far field of the vortex is surrounded by normalized concentrations of $\xi = 1.0$ or 0. In a given domain with far-field concentrations of $\xi = 0$ and 1.0, the value of f varies between 0 for completely unmixed region (i.e. $\xi = 0$ or 1.0 everywhere) and 1.0 for 1:1 mixing in which case $\xi = 0.5$ throughout the domain. The area over which the integration is carried out is selected here to allow comparisons of the mixedness for different vortices. In this study, the domain A was selected as the whole extent of the imaging region in the x-direction (17.0 cm) and 1.2 times the vertical extent ($2r_*$) of the largest vortex considered in the y-direction (7.4 cm).

Figure 14(*a*) shows the mixedness parameter as a function of time for three vortices. Mixedness increases linearly with time and its rate of change becomes larger with

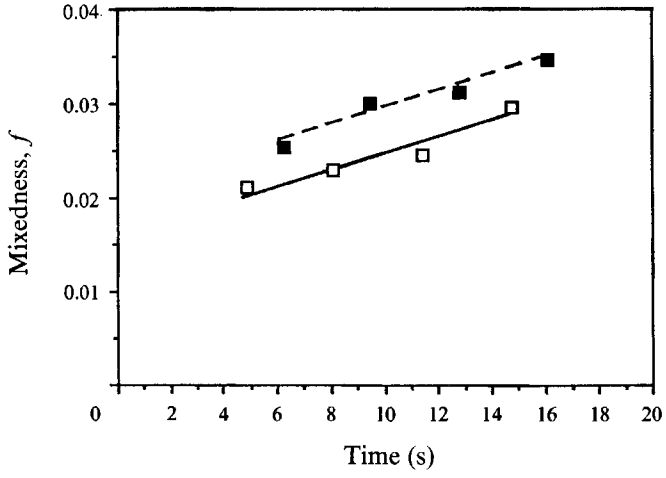

FIGURE 15. Mixedness as a function of time from the dilution experiments: □, $\Gamma = 3.05$ cm^2/s (penetrated fluid with dye); ■, $\Gamma = 2.99$ cm^2/s (penetrating fluid with dye).

increasing vortex circulation. The initial value of mixedness is that of the diffusion layer prior to vortex generation. The same results were replotted in figure 14(*b*) as a function of vortex circulation–time product. The mixedness is seen to be well correlated with Γt for all vortex strengths. Figure 15 shows the insensitivity of the rate of mixing to the manner in which the vortical structure is initiated. It shows that the only effect of the vortex initiation asymmetry on mixedness is a shift in its value with the same rate of growth.

Another measure relevant to molecular mixing is the scalar dissipation, defined by

$$\nabla\xi \cdot \nabla\xi = \left(\frac{\partial\xi}{\partial x}\right)^2 + \left(\frac{\partial\xi}{\partial y}\right)^2. \tag{15}$$

The relationship of scalar dissipation to mixing can be explained through the convection–diffusion equation of a scalar:

$$\left(\frac{\partial}{\partial t} - \boldsymbol{u}\cdot\nabla - D\nabla^2\right)\xi = 0, \tag{16}$$

where ∇ and ∇^2 are the gradient and Laplacian operators, $\boldsymbol{u}$ is the velocity vector and D is the mass diffusivity. The scalar energy equation can be obtained utilizing (16) as

$$\left(\frac{\partial}{\partial t} - \boldsymbol{u}\cdot\nabla - D\nabla^2\right)\tfrac{1}{2}\xi^2 = -D\nabla\xi\cdot\nabla\xi. \tag{17}$$

This equation relates the changes in the scalar energy distribution as a result of convection, diffusion and the scalar dissipation term on the right-hand side. Scalar dissipation is seen to be the only mechanism with which the scalar energy in the field is dissipated. In our experiments, the spatially averaged values of scalar dissipation,

$$\bar{S} \equiv \frac{1}{A}\int_A (\nabla\xi\cdot\nabla\xi)\,\mathrm{d}A, \tag{18}$$

were computed as a function of vortex strength and time. Results shown in figure 16(*a*) indicate that scalar dissipation also varies linearly with time. The same results were replotted in figure 16(*b*), showing a linear dependence on the Γt product. These results

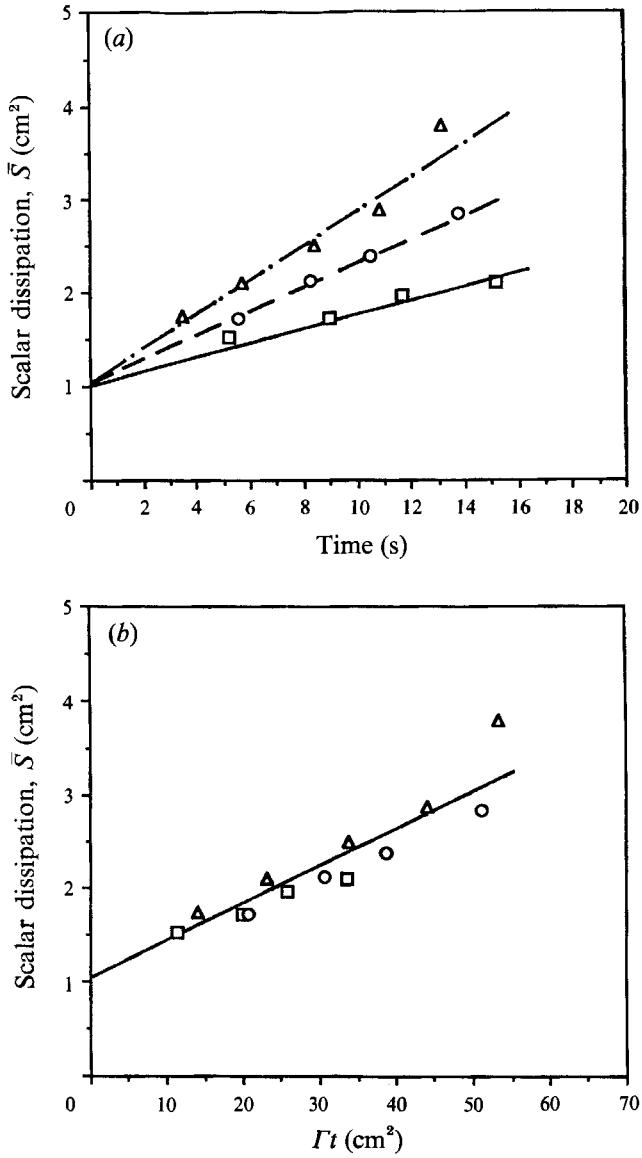

FIGURE 16. Spatially averaged scalar dissipation as a function of (*a*) time and vortex strength and (*b*) vortex circulation–time product, Γt from the dilution experiments. Symbols as figure 13.

indicate that the dissipation of concentration stratifications in the field of a vortex are enhanced with increasing vortex strength and time in a rather simple way, i.e. linearly.

These results can now be discussed in terms of the two effects that influence mixing enhancement, namely increase of contact area between the mixing streams and the augmentation of diffusion flux across the stretching diffusion layers. First considering the deformation of a material segment initially situated along the straight interface separating the two scalar half-planes, dr, in the field of a potential vortex, the increase in the length of this segment can be written as

$$\frac{\mathrm{d}l}{\mathrm{d}r} = \left[1 + \left(\frac{\Gamma t}{2\pi r^2}\right)^2\right]^{\frac{1}{2}} \approx \frac{\Gamma t}{2\pi r^2}, \tag{19}$$

where dl is the deformed length of the material segment whose original length was dr. For large values of $\Gamma t/\pi r^2$, the last expression approximates this change in length. Integrating this relation for an initial length between r_{min} and r_{max}, one obtains

$$\frac{l}{r_{max}-r_{min}} = \frac{\Gamma t}{2\pi r_{min} r_{max}}. \tag{20}$$

The increase in contact area between the two fluids is thus proportional to Γt based on this simple analysis. The linear dependence of the experimental mixing results on Γt suggest that mixing enhancement is, to a large extent, a consequence of the contact area increase between the two fluids in the vortex. The contribution of augmented mass diffusion rate, as a result of steepening of concentration gradients during stretch is expected to play a small role in low-mass-diffusivity media like liquids or in the high-Schmidt-number limit. The linear dependence of mixing enhancement on vortex strength and time is also in agreement with a theoretical study of Cetegen & Sirignano (1990) which covered a wide range of vortex strengths and Schmidt numbers.

5.2. *Chemical reaction experiments*

The PLIF images generated in the chemical reaction experiments are characteristically different in appearance as compared to the dilution experiments since fluorescence only appears in regions of molecular diffusion. Figure 17 (plate 2) shows the colour-coded background-corrected concentration images at two instants for one vortex. In these experiments, the free-stream acid and base concentrations were selected such that the fluorescence threshold occurred at a small value of the base volume fraction ($\xi_s = 0.05$) allowing essentially the whole spectrum of mixture fractions ($0.05 < \xi \leqslant 1.0$) to be detected. Since the fluorescence intensity is linearly proportional to the product concentration, these images reveal directly the product concentration distributions. The reaction product is formed in spiralling diffusion layers in the vortex, penetrating towards the vortex core. Since the product can only form upon molecular diffusion of reactants into one another, the image highlights the extent and distribution of the molecularly diffused fluids.

In a similar manner to the dilution experiments, the variation of the mean normalized product concentration, C_{rm}/C_{d0} was also computed in the reacting vortex. C_{rm} is defined as

$$C_{rm}(y;\xi_s \to 0) = \int_0^1 C_p(\xi;\xi_s \to 0)\, P(\xi, y)\, d\xi. \tag{21}$$

In contrast to its dilution counterpart, this is a measure of molecularly mixed fluid or the amount of product in the vortical structure. $\xi_s \to 0$ implies that essentially all mixture fractions are included in this definition. $P(\xi, y)$ is the probability density function. Figure 18 shows an example of C_{rm} variation with y at two different instants of time for one vortex strength. The concentration of the molecularly mixed fluid becomes larger with increasing time. There also appears to be large variations in the average product concentration through the centre of the vortex, and the highest concentrations occur near the vortex cores.

The amount of product in the whole region can be found by integration:

$$\bar{C}_{rm} = \frac{1}{2y_m}\int_{-y_m}^{+y_m} C_{rm}(y;\xi_s \to 0)\, dy. \tag{22}$$

This parameter is plotted in figure 19 as a function of Γt for a number of vortices. The

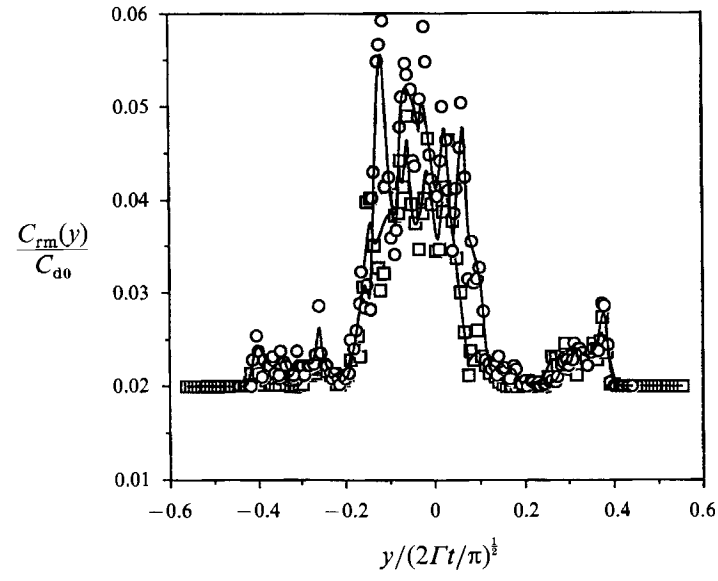

FIGURE 18. Variation of the normalized product concentration as a function of the y-coordinate for the chemically reacting vortex at $\Gamma = 4.59$ cm^2/s; □, $t = 6.4$ s; ○, $t = 10.1$ s.

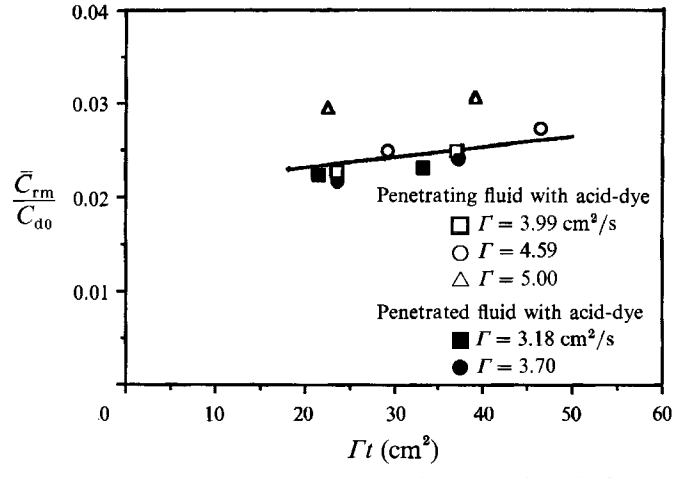

FIGURE 19. Amount of product integrated over the entire domain for the chemically reacting vortices.

amount of product in the vortex appears to increase linearly with Γt for all vortices, with one vortex having higher values. This finding is in good agreement with the dilution experiments, indicating its validity in the molecular mixing limit.

Mixedness factor, f, computed in a similar manner to the dilution experiments is shown in figure 20. In the chemically reacting experiments, ξ is defined as the base volume fraction and it was computed over the same domain as in the dilution experiments. These results, representing mixedness at infinite resolution, are similar to those from the dilution experiments, indicating that mixedness depends linearly on both time and vortex strength and also the Γt product. The major difference between these and the dilution experiment is the resolution of mixing scales. In the chemical reaction experiment, mixing at the molecular diffusion scales is highlighted. A

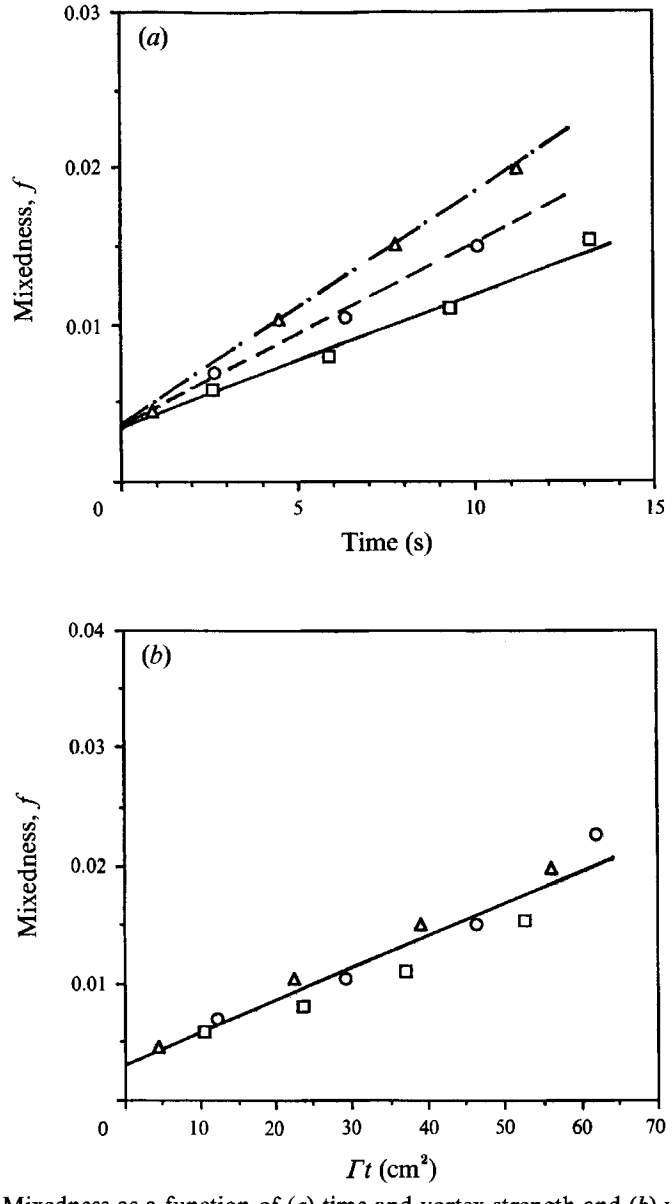

FIGURE 20. Mixedness as a function of (*a*) time and vortex strength and (*b*) vortex circulation–time product, Γt from the chemical reaction experiments: □, $\Gamma = 3.99$ cm²/s; ○, $\Gamma = 4.59$ cm²/s; △, $\Gamma = 5.00$ cm²/s.

comparison of the two sets of data is given in figure 21. The values of mixedness as well as the rate of change with respect to Γt appear to be somewhat higher for the dilution experiments as compared to those from the reaction experiments, although the linear dependence persists. This difference is primarily due to the inclusion of mixing scales larger than molecular diffusion in the dilution experiments. In this context, the chemical reaction experiments provide more accurate estimates of molecular diffusion since they are not affected by the scale resolution problem.

The two measures of mixing discussed above, namely mixedness and scalar dissipation, are related to one another. This relationship can be obtained upon spatial

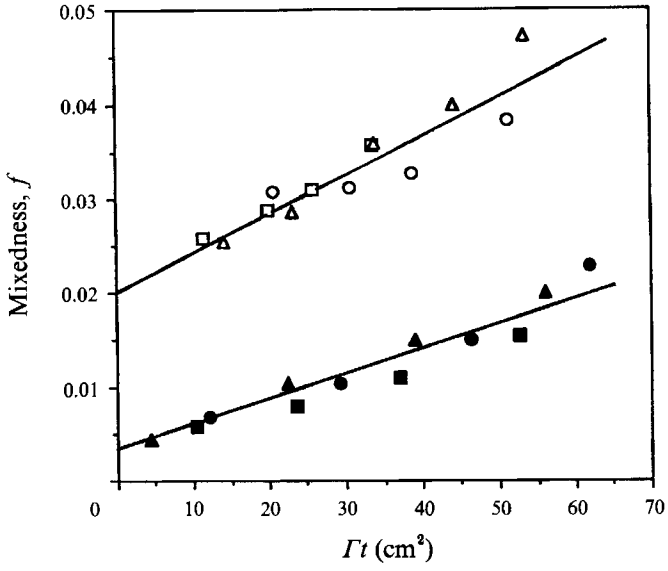

FIGURE 21. Comparison of mixedness from dilution (open symbols) and chemical reaction (solid symbols) experiments.

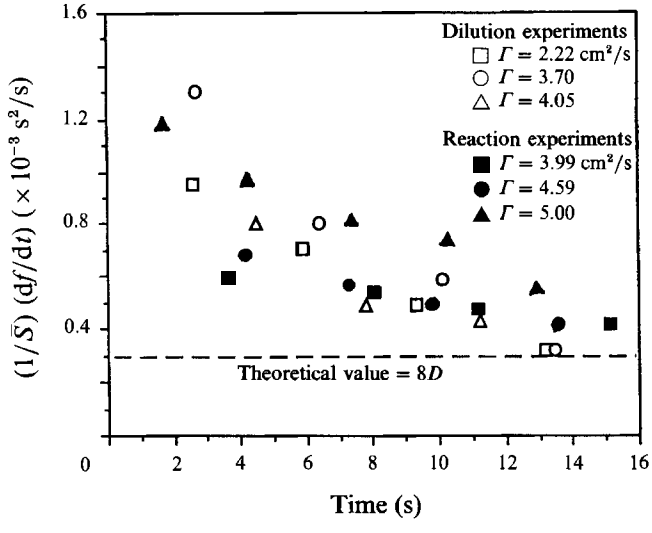

FIGURE 22. Rate of change of mixedness normalized by spatially averaged scalar dissipation as a function of time for reacting and non-reacting vortices with differing circulation.

integration of the scalar energy equation (17) and noting that the diffusion term on the left integrates to zero provided that the integration domain extends outside the mixing zone. It can be shown that

$$df/dt = 8D\bar{S} \tag{23}$$

in the quasi-steady limit. Figure 22 shows the variation of the rate of change of mixedness normalized by the spatially averaged scalar dissipation as a function of time for a number of experiments. It is seen that the experimental results asymptotically approach this relation at long times, for which the quasi-steady approximation is considered to be valid.

6. Concluding remarks

A unique experimental method for generating single laminar vortices along a diffusion layer has been described and used to quantify large- and small-scale mixing in the field of the generated vortices. Using planar laser-induced fluorescence measurements of scalar concentration fields, several measures of stirred fluid distributions and molecular diffusion have been obtained as a function of vortex strength and time of growth. The results have been discussed in the light of mechanisms of mixing enhancement in a vortical flow field. The results are summarized below for large- and small-scale mixing.

The large-scale mixing measures are pertinent to redistribution of the initial concentration field at larger than molecular diffusion scales under the influence of a vortex. Firstly, the stirred fluid mixture fraction profiles across the vortices studied show approximate self-similarity in their spatial variation with respect to vortex circulation–time product as $(\Gamma t)^{-\frac{1}{2}}$ which is the inverse characteristic lengthscale in an inviscid vortex. The stirred fluid fractions, integrated over the whole mixing region, are found to be linearly dependent on the Γt product for a range of these parameters. The probability density distributions exhibit two characteristic peaks at the free-stream concentrations with small intermediate mixture probabilities that evolve with time.

The two measures of molecular diffusion, namely mixedness and spatially averaged scalar dissipation, vary linearly with the vortex circulation and time product. The factors contributing to mixing enhancement, in the presence of a vortex, are expected to be the contact area generation between the two fluids and the mass diffusion rate augmentation across stretched diffusion layers. A simple estimate shows that the contact area between mixing fluids in a potential vortex grows linearly with the Γt product. The experimental results presented also exhibiting this dependence point towards the conclusion that the main contribution to mixing enhancement results from the increase in the contact area along the diffusion layers. The mixing enhancement appears to be dominated by the contact area generation for liquids or the high-Schmidt-number ($Sc = \nu/D$) limit. However, the diffusion rate enhancement will be more pronounced in diffusive fluids such as in gases. Furthermore, viscous regions of the vortex will be involved in fluid deformations and also in the resultant scalar mixing.

Finally, the vortex generation method described here can be extended to mixing in multiple vortex configurations by sequential generation. These studies, such as on vortex couples, complement those on other vortex systems like vortex pairs (Southerland *et al.* 1990) and other prototypical flow fields. The method also provides a potential way of looking at mutual interactions of two or more vortices.

This research was sponsored by a grant from the University of Connecticut Research Foundation. BMC acknowledges the illuminating discussions with C. H. K. Williamson and J. C. Bennett. Skillful help of Peter Boardman in the laboratory was greatly appreciated during these experiments.

REFERENCES

BATCHELOR, G. K. 1967 *An Introduction to Fluid Dynamics.* Cambridge University Press.

BREIDENTHAL, R. E. 1981 Structure in turbulent mixing layers and wakes using a chemical reaction. *J. Fluid Mech.* **109**, 1–24.

BROWN, G. L. & ROSHKO, A. 1974 On density effects and large scale structure in turbulent mixing layers. *J. Fluid Mech.* **64**, 775–816.

CARRIER, G. F., FENDELL, F. E. & MARBLE, F. E. 1975 The effect of strain rate on diffusion flames. *SIAM J. Appl. Maths* **28**, 463–500.

CETEGEN, B. M. & SIRIGNANO, W. A. 1990 Study of mixing and chemical reaction in the field of a vortex. *Combust. Sci. Tech.* **72**, 157–181.

FENDELL, F. E. 1965 Ignition and extinction in combustion of initially unmixed reactants. *J. Fluid Mech.* **21**, 281–303.

KARAGOZIAN, A. R. & MARBLE, F. E. 1986 Study of mixing and reaction in the field of a vortex. *Combust. Sci. Tech.* **45**, 65–84.

KOOCHESFAHANI, M. M. & DIMOTAKIS, P. E. 1986 Mixing and chemical reactions in a turbulent liquid mixing layer. *J. Fluid Mech.* **170**, 83–112.

LAVERDANT, A. M. & CANDEL, S. M. 1989 Computation of diffusion and premixed flames rolled-up in vortex structures. *J. Prop. Power* **5**, 139.

MARBLE, F. E. 1985 Growth of a diffusion flame in the field of a vortex. In *Recent Advances in Aerospace Sciences*, vol. 19 (ed. C. Casci), pp. 395–413. Plenum.

MARBLE, F. E. 1988 Mixing, diffusion and chemical reaction of liquids in a vortex field. In *Chemical Reactivity in Liquids* (ed. M. Moreau & P. Turq). Plenum.

MARBLE, F. E. & BROADWELL, J. E. 1977 The coherent flame model for turbulent chemical reactions. *Project SQUID Tech. Rep.* TRW-9-PU.

MOHAMAD, N. 1991 An experimental study of mixing and chemical reaction in a vortex. Master of Science Thesis, University of Connecticut, Storrs.

MUNGAL, M. G. & HOLLINGSWORTH, D. K. 1989 Organized motion in a very high Reynolds number jet. *Phys. Fluids* A **1**, 1615–1623.

OTTINO, J. M. 1982 Description of mixing with diffusion and reaction in terms of the concept of material surfaces. *J. Fluid Mech.* **114**, pp. 83–103.

OTTINO, J. M. 1989 *The Kinematics of Mixing: Stretching, Chaos and Transport.* Cambridge University Press.

PETERS, N. & WILLIAMS, F. A. 1988 Premixed combustion in a vortex. *Twenty-Second Symposium (Intl) on Combustion*, pp. 495–503. The Combustion Institute.

RANZ, W. E. 1977 In *Mixing of Liquids by Mechanical Agitation* (ed. J. J. Ulbrecht & G. K. Patterson). Gordon and Breech.

RANZ, W. E. 1979 Application of a stretch model to mixing, diffusion and reaction in laminar and turbulent flows. *AIChE J.* **25**, 41–47.

REHM, R. G., BAUM, H. R., LOZIER, D. W. & ARONSON, J. 1989 Diffusion-controlled reaction in a vortex field. *Combust. Sci. Tech.* **66**, 293–317.

SOUTHERLAND, K. B., PORTER, J. R., DAHM, J. A. & BUCH, K. A. 1991 An experimental study of the molecular mixing process in an axisymmetric laminar vortex ring. *Phys. Fluids* A **3**, 1385.